

Numerical analysis of fibre reinforced polymer retrofitted masonry panels



Bibiana Luccioni^{a,*}, Viviana C. Rougier^b

^a Structures Institute, National University of Tucumán, CONICET, Av. Independencia 1800, 4000 S.M. de Tucumán, Argentina

^b Group of Numerical Methods, Reg. Fac. Concepción del Uruguay, National Technological University, Ing. Pereira 676, 3260 Concepción del Uruguay, Argentina

ARTICLE INFO

Article history:

Received 27 February 2009

Revised 26 September 2012

Accepted 22 October 2012

Keywords:

Masonry

Fibre reinforced polymer

Retrofitting

Mechanical behaviour numerical model

ABSTRACT

The numerical analysis of the in-plane mechanical behaviour of unreinforced and carbon fibre reinforced polymer (CFRP) retrofitted masonry walls, using a coupled damaged-plasticity model, is presented in this paper. The comparison of numerical and experimental results shows the model ability to simulate the in-plane behaviour of masonry elements retrofitted with CFRP. Numerical analyses are carried out to verify the efficiency of the reinforcement with CFRP. Finally, the in-plane behaviour of real scale retrofitted walls is reproduced.

© 2012 Elsevier Ltd. All rights reserved.

1. Introduction

The life span of a masonry structure can be over a 1000 years if designed and constructed properly. However, there are several masonry buildings that have been damaged in a shorter time than expected due to different external actions like earthquakes, impact loads, change of use or aggressive agents. Many of this masonry structures are historical buildings that should be preserved as cultural heritage.

Masonry structures failure is generally preceded by a massive cracking development in the mortar joints. For this reason, the mortar joints limit the final strength. Depending on compression degree, failure can take place only in the joints, or a combined crack brick–mortar joint can occur. Failure is normally brittle and sudden. One way of preventing this type of problem is through FRP reinforcement. This reinforcement can be done covering the entire wall with fabrics of carbon or glass impregnated in epoxy resin or through strips applied in the same way. Before applying the FRP laminates, the specimen surfaces must be thoroughly cleaned from mortar protrusions and dust using a wire brush and air blasting. The pre-cut fabrics are then placed on previously primed surfaces and more epoxy is applied to ensure complete fabric saturation (wet process) [1–4].

The reinforcement and rehabilitation technique with fibre reinforced polymers (FRPs) has experimentally proved to be very effective. If the reinforcement is properly designed this technique may enhance the in-plane behaviour, increasing ductility and in some cases, ultimate strength and stiffness [1–6].

The numerical assessment of solid clay unreinforced masonry panels, panels retrofitted with carbon fibre reinforced polymer (CFRP) laminates and full scale unreinforced and retrofitted walls is presented in this paper. The numerical model used results from a proper combination of numerical models previously developed by the authors. Moreover, two different approaches using the same model are presented: a micro and a macro-approach. First, a micro-approach in which bricks, mortar and CFRP bands are distinguished is proposed and calibrated with the experimental results of unreinforced masonry unities presented in Ref. [4]. Then, this type of model is shown to be able to reproduce results of several retrofitted masonry specimens from that experimental program. Additionally, a macro-approach in which average properties of masonry are obtained from a numerical homogenisation procedure is proposed and used for the numerical simulation of full scale retrofitted masonry walls tested by other authors under combined vertical and horizontal cyclic load [7,8]. The comparison with experimental results shows the ability of the numerical model to reproduce the hysteretic response of CFRP retrofitted masonry under in plane cyclic load.

First, a brief description of the existent models for masonry retrofitted with FRP composites is presented. Then, the model used in this paper is described and the main coupled damaged-plasticity orthotropic model equations used are developed [9–11]. Numerical results are compared with experimental tests carried out over

* Corresponding author. Address: Country Las Yungas, 4107 Yerba Buena, Argentina. Tel./fax: +54 381 4364087.

E-mail addresses: bluccioni@herrera.unt.edu.ar (B. Luccioni), rougier@frcu.unt.edu.ar (V.C. Rougier).

URLs: <http://www.herrera.unt.edu.ar/iest> (B. Luccioni), <http://www.frcu.unt.edu.ar> (V.C. Rougier).

small solid clay masonry panels retrofitted with CFRP using different layouts subjected to compression normal to bed joints and diagonal compression tests [3,4]. Finally, the same model is also used for the analysis of actual size walls behaviour [7,8]. The walls, reinforced with FRP, were subjected to in-plane constant vertical load and lateral cyclic load. The capability of the model is proved and the efficiency of different retrofitting schemes is compared.

2. Experimental results

Some authors have studied the behaviour of reinforced masonry under compression normal and parallel to bed joint [4,12,13]. Shear behaviour of FRP retrofitted and repaired masonry was also studied by many authors [1–3,5–8,12–25].

2.1. Compression behaviour

According to a research carried out by El-Dakhkhni et al. [12] on small masonry specimens made with hollow concrete blocks subjected to uniaxial compression normal and parallel to the bed joint, the reinforcement with FRP not only increases the strength but also increases the ductility preventing out of plane brittle failure and keeping the wall integrity even after significant structural damage. Prakash and Alagusundaramoorthy [13] studied the effectiveness of glass fibre reinforced polymers (GFRPs) retrofitting on the behaviour of masonry wall specimens constructed with high stiffness cement mortar and low stiffness bricks and subjected to compression normal and parallel to bed joint. GFRP retrofitting increased the strength and stiffness of the wall specimens but the average ultimate strain was significantly reduced.

2.2. Shear behaviour

Zhuge [14] recently presented a review describing the research on shear strengthening of FRP-retrofitted unreinforced masonry walls. Shear behaviour of FRP retrofitted clay masonry has been studied at different scales: small specimens made of three bricks [15,16,25]; small panels under diagonal compression [2,12,17]; and half scale [18,19] actual scale walls [5,7,8,20,22], under combined vertical and lateral load simulating seismic action.

Some authors have experimentally studied shear behaviour at elementary level [15]. Ehsani et al. [25], Roca and Araiza [15] and Luccioni and Rougier [16], among others, investigated the efficiency of external shear reinforcement of small specimens made by three solid bricks and two joints. The retrofitting with unidirectional CFRP bands oriented orthogonally to the joints increases the shear strength. The anchorage length of the CFRP band is a very important variable in the design of the shear reinforcement. Strength increases with the length of the bands. In general, the failure is produced by the failure of the bricks surface producing the debonding of the CFRP laminas.

El-Dakhkhni et al. [12] investigated the effects of FRP laminates on altering the failure mode and strength and deformation characteristics of hollow concrete small specimens subjected to diagonal tension and joint shear. They concluded that laminates significantly increased the load-carrying capacity of the masonry assemblages exhibiting shear failure along the mortar joints. The average joint shear strength of the retrofitted specimens was equal to eight times that of their unreinforced counterparts. The values of the coefficients of variation for the retrofitted assemblages were generally lower than those of the unreinforced specimens. This result demonstrates the laminate's role in reducing strength anisotropy and variability of unreinforced masonry.

Valluzzi et al. [2] and Gabor et al. [17] performed the diagonal compressive tests to investigate the in-plane shear response of

small brick masonry panels strengthened with FRP laminates. From the results obtained by Valluzzi et al. [2] and Gabor et al. [17] on panels made of solid and hollow clay bricks, respectively, it can be concluded that fibre reinforced polymer reinforcement increases shear strength and ductility depending on the reinforcement scheme. It increases the stiffness, especially in solid brick masonry and prevents brittle failure only for specimens with the reinforcement covering all their surfaces.

ElGawady et al. [18,19] studied the response of half scale masonry panels strengthened with FRP laminates applied diagonally to the joints subjected to both static and cyclic loading. The increase in the lateral strength was proportional to the amount of FRP axial rigidity. However, the use of high amount of FRP axial rigidity led to very brittle failure. Many researchers have also studied the seismic reinforcement with fibre reinforced polymers of full-scale [5,7,8,20,22] masonry walls made of hollow clay bricks. It was observed that the reinforcement improves lateral stability of the walls [14], increases the shear strength of the walls, the maximum displacement before failure, and the displacement and load of first major crack [7]. Seismic retrofitting of unreinforced masonry walls with FRP proved to be an effective and reliable strengthening alternative [21,23,24].

Although experimental results have shown the advantages of this retrofitting technique, analytical or numerical tools for description of the mechanical behaviour of unreinforced and reinforced masonry elements under different load conditions are needed to improve this intervention technique.

The behaviour of reinforced masonry is complex and the degradation and failure mechanisms depend on mechanical properties, mainly on the elastic properties and on the strength of the mortar, of the blocks or bricks and of the laminate and on the particular retrofitting schemes used.

It can be noted that for any type of loading condition, the mortar is the first component to fail. After complete degradation of the mortar, a composite made of blocks connected by the laminate is obtained. Thus, strain concentrations between adjacent blocks occur. On the other hand, as the blocks can support reduced tensile stresses, they fail and produce laminate debonding before it can experiment high deformations.

3. Brief review of numerical models for FRP reinforced masonry

Numerical simulation of the behaviour described in previous section is not a simple task, and even though in the last years there has been more research on it [17,25–31], the existing numerical tools are still rather limited.

Numerical models used for FRP reinforced or retrofitted masonry usually involve masonry models. As models used for all composite materials, masonry models can be classified in three types [28].

- *Micro-models*: Mortar, bricks and their interfaces are independently simulated using different constitutive models appropriate for each material with properties obtained from experimental tests performed on individual bricks, masonry units or special brick–mortar small elements designed to test the brick mortar interface. This type of model is able to reproduce experimental tests on small masonry elements but has high computational cost when applied to full scale masonry walls or buildings.
- *Micro–macro*: Different models are considered for bricks, mortar and interfaces combined with some kind of homogenisation procedure to obtain an equivalent homogeneous model for structural analysis. This type of model has the advantage of reducing the computational cost without requiring too much experimental data.

- *Macro-models*: A phenomenological constitutive law is used to model masonry behaviour. The stress strain relationships are obtained from experimental tests performed on small masonry units subjected to different types of loads. While very simple to use in structural analysis, this type of model requires many experimental tests that should be repeated for each type of masonry although the bricks and the mortar are the same.

These different approaches combined with different ways of modelling the FRP reinforcement have also been used to model FRP retrofitted masonry.

Ehsani et al. [25] used a commercial finite element code to assess the effectiveness of the FRP retrofitting in the enhancement of masonry shear strength. They assumed linear elastic behaviour for the bricks and the composite and obtained a good numerical solution when the fibres were placed at 45° for which the experimental response was linear but not for other inclinations.

Cecchi et al. [26] developed a numerical model based on homogenisation theory for the simulation of the in-plane and out-of-plane behaviour of CFRP retrofitted masonry. They proposed two alternative homogenisation processes: an analytical multi-step method and a numerical one step method. These models were not compared with experimental results in the paper [26].

Gabor et al. [17,27] presented three different finite element approaches developed with a commercial code for the analysis of unreinforced and FRP retrofitted masonry walls under in plane loading. The detailed model considers the real configuration of the masonry panels (constituted from bricks and mortar) and the composite reinforcement. This modelling was applied in both cases (unreinforced and strengthened panels). A simplified model, considering the experimentally measured global mechanical parameters of the masonry panels and a simplified model, based on homogenisation theory, where bricks and mortar were replaced by an equivalent continuum, were used for the analysis of unreinforced masonry. They concluded that the finite element modelling can be a useful tool for the design of FRP reinforcement. A good correlation between experimental results and numerical results using homogenisation models for unreinforced masonry was found. Since detailed models used for retrofitted masonry required a high computational cost, the further development of a homogenisation model for retrofitted masonry was recommended.

Grande et al. [28] presented two different approaches able to model the behaviour of unreinforced and reinforced masonry structures. The first one was based on a micro-mechanical and multi-scale analysis combined with the use of the kinematic and static theorems of the limit analysis. FRP–masonry interaction was simulated with a rigid-perfectly plastic model. The second approach was based on a macroscopic model. A smeared crack approach was used for masonry. Moreover, different modelling strategies and constitutive laws were adopted for the FRP-reinforcement taking into account the delamination phenomenon. FRP strips were modelled using truss elements directly connected to the nodes of the mesh of the panels. Both experimental failure loads and load–displacement curves were satisfactorily reproduced with all the adopted models. However, the post-peak behaviour was captured well only when brittle phenomena were taken into account. The simplified approach proposed to consider the contribution of the reinforcement was able to reproduce the delamination process of the FRP strengthening when the strips were not mechanically fixed to the masonry support and the delamination process started from the free edges of the strips. The authors suggested that a different model should be chosen when the ends of the FRP strips were mechanically fixed to the surface of the panels.

A heterogeneous model at the meso-scale has been used by Fedele and Milani [29] for the interpretation of delamination tests

on FRP-reinforced masonry pillars. Brick and mortar were modelled independently, with different damage variables and activation criteria in tension and compression. A perfect adhesion has been assumed between the FRP external sheet and the masonry support. Numerical results in terms of equivalent interface behaviour satisfactorily agreed with the prediction of the design formulae suggested by the CNR Italian norm. The authors recommended the development of a three-dimensional (3D) extension of the model in order to take into account effects neglected in the proposed bi-dimensional idealisation. These effects are expected to influence the overall response and collapse mechanisms in delamination tests.

Milani et al. [30] developed a 3D homogenised FE limit analysis software for the numerical prediction of collapse loads and failure mechanisms of entire masonry buildings reinforced with FRP strips. In a first step failure surfaces for homogenised unreinforced masonry were obtained. In this step rigid-infininitely resistant wedge-shaped 3D elements and 3-noded rigid-infininitely resistant elements were used for masonry and FRP strips respectively. Delamination phenomenon of the strips from the support was considered imposing to FRP–masonry interfaces a limited resistance. Good agreement between numerical results and available data was found.

Different approaches were used by Su et al. [31] to model FRP reinforced walls under out-of-plane loading. They differ in the way that the masonry was modelled using a homogenised model, a smeared-crack model and a discrete model. In all cases the interface between the reinforcement and masonry was simulated using 1 mm interface elements with bilinear behaviour. Good agreement with experimental results from small scale pull out tests was found using the three models. The homogenised model together with the interface element model was then used to simulate the response of full-scale masonry walls damaged under cyclic out-of-plane loading and then repaired with CFRP and reloaded. Numerical results agreed with experimental results.

4. Proposed model

Masonry is considered to be a composite material built of brick units and mortar joints. In this paper two different approaches were considered to model masonry itself. First the masonry and CFRP reinforced masonry elements under compression normal to bed joints and diagonal compression are simulated with a micro-model in which bricks and mortar are separately modelled.

The application of this model to masonry requires the proper definition of the finite element model and the definition of several functions (yield function, potential function, damage function, hardening functions, etc.) and parameters for the constitutive models. Functions normally used for concrete were used for bricks and mortar. Some of the mechanical properties of bricks and mortar, like elasticity modulus, Poisson ratio, compression strength, tension strength, fracture energy and compression strain hardening were obtained from tests performed on bricks and mortar specimens [3]. The rest of the parameters were indirectly obtained through numerical simulation of small unreinforced masonry specimens and comparison with experimental results [4].

The interface between bricks and mortar allowing possible debonding is also approximately considered without explicitly modelling the interface but properly modifying the mortar constitutive equation [16,32]. The mortar was supposed to be anisotropic with reduced shear strength in the interface plane. The value of the shear strength was adjusted to reproduce the experimental results of small masonry specimens tested in [16].

Once this approach to model masonry is calibrated and validated, a numerical homogenisation, in which the average proper-

ties of masonry are numerically obtained with the previous micro-model, is performed. Then an equivalent homogeneous anisotropic plastic damage model with those properties is used to simulate the behaviour of full scale walls.

In both approaches FRP reinforcement is simulated without explicitly modelling reinforcement elements but with a generalisation of the classic mixture theory [33]. In this way, FRP reinforced bricks or FRP reinforced mortar in the micro-approach or FRP reinforced masonry in the homogenised approach are considered as composite materials made of bricks, mortar or masonry and FRP composite respectively. The mixture theory is applied to these composites and the modified mixture theory is used for the FRP composite itself [34,35].

4.1. Constitutive model for solid clay bricks, mortar and homogenised masonry

An orthotropic plastic-damage model [36,9–11] is used for bricks and mortar in the micro-model. The same model is applied to the simulation of masonry as a homogenised material. Even though different materials with different mechanical properties are dealt with, solid clay bricks, mortar and masonry are frictional materials, that is, their behaviour is influenced by hydrostatic pressure. Bricks are normally made of isotropic materials and mortar is also approximately isotropic. However, mortar and bricks are modelled as orthotropic materials in order to account for the weakness of the interfaces and the possibility of relative displacements without explicitly modelling the interfaces [32]. Thus the same general coupled elasto-plastic damage model for orthotropic materials, but with different material constants and functions [8] is used for bricks, mortar and masonry in the homogenised approach.

4.1.1. Anisotropy treatment

The anisotropic model is based on the hypothesis that there are two spaces [36,7]: (a) a real anisotropic space and (b) a fictitious isotropic space. The problem is solved in the fictitious isotropic space which allows the use of elasto-plastic and damage models developed for isotropic materials.

The stress tensors in both spaces are related by means of a transformation defined as follows:

$$\tau_{ij} = A_{ijkl}(\sigma_{ij}; \kappa^p) \sigma_{kl} \quad (1)$$

where τ_{ij} and σ_{kl} are the stress tensors in the spaces (b and a) respectively and A_{ijkl} is a fourth order transformation tensor that has the information about the strength anisotropy. In general, this tensor is a function of the stress state and of the evolution of the elasto-plastic process defined by internal variables like the plastic damage variable κ^p [10] that is the isotropic plastic hardening variable. All the components' materials are assumed to be initially orthotropic in this paper. There are different alternatives to define tensor A_{ijkl} for this case [9,37–40]. The simplest way is a diagonal fourth order tensor [7],

$$A_{ijkl} = \sum_{m=1}^3 \sum_{n=1}^3 \delta_{im} \delta_{jn} \delta_{km} \delta_{ln} \tau_{mn} / \sigma_{mn} \quad (2)$$

The threshold that marks the beginning of plastic or damage behaviour is defined by means of a yield or damage function:

$$F(\sigma_{ij}; \alpha) = \bar{F}(\tau_{ij}; \bar{\alpha}) = 0 \quad (3)$$

where F and \bar{F} designate the yield or damage functions in the real anisotropic and fictitious isotropic spaces respectively and α and $\bar{\alpha}$ are internal variables corresponding to such spaces.

The spaces transformation defined in Eq. (1) allows the use of yield or damage functions \bar{F} defined for isotropic materials in the fictitious isotropic space. It should be noted that such isotropic

space is isotropic with respect to plastic or damage thresholds, but not necessarily regarding other properties, such as the elastic stiffness.

The plastic deformation in the real space is calculated by means of the following flow rule

$$\dot{\varepsilon}_{ij}^p = \dot{\lambda} \frac{\partial G}{\partial \sigma_{ij}} \quad (4)$$

where G is the potential function defined in the actual stress space. Instead of working with this function that should be anisotropic, it is possible to work with a potential function \bar{G} , defined in the fictitious isotropic space

$$G(\sigma_{ij}; \alpha) = \bar{G}(\tau_{ij}; \bar{\alpha}) \quad (5)$$

Then, Eq. (4) is written,

$$\dot{\varepsilon}_{ij}^p = \dot{\lambda} \frac{\partial G}{\partial \sigma_{ij}} = \dot{\lambda} \frac{\partial \bar{G}}{\partial \tau_{kl}} \frac{\partial \tau_{kl}}{\partial \sigma_{ij}} = \dot{\lambda} \frac{\partial \bar{G}}{\partial \tau_{kl}} H_{kl ij} \quad \text{with} \quad H_{kl ij} = \frac{\partial \tau_{kl}}{\partial \sigma_{ij}} \quad (6)$$

4.1.2. Isotropic model: general form

The total free energy density per unit volume Ψ can be assumed to be formed by two independent parts: the elastic part Ψ^e and the plastic part Ψ^p . For infinitesimal strains and thermally stable problems, the elastic part of free energy density Ψ^e is written as a quadratic function of the elastic deformation tensor ε_{ij}^e ,

$$\Psi^e = \frac{1}{2} \varepsilon_{ij}^e C_{ijkl}^e \varepsilon_{kl}^e = \frac{1}{2} \varepsilon_{ij}^e (1-d) C_{ijkl}^0 \varepsilon_{kl}^e = (1-d) \Psi^o \quad (7)$$

$$\Psi^o = \frac{1}{2} \varepsilon_{ij}^e C_{ijkl}^0 \varepsilon_{kl}^e \quad \varepsilon_{ij}^e = \varepsilon_{ij} - \varepsilon_{ij}^p$$

where C_{ijkl} is the secant constitutive tensor affected by the evolution of damage, C_{ijkl}^0 is the stiffness tensor of the virgin material, d is the scalar damage variable used to model stiffness degradation, Ψ^o is the elastic free energy density for the virgin material, ε_{ij} is the strain tensor and ε_{ij}^p is the plastic strain tensor.

The secant constitutive equation results

$$\sigma_{ij} = \frac{\partial \Psi}{\partial \varepsilon_{ij}^e} = C_{ijkl} \varepsilon_{kl}^e = (1-d) C_{ijkl}^0 \varepsilon_{kl}^e = (1-d) C_{ijkl}^0 (\varepsilon_{kl} - \varepsilon_{kl}^p) \quad (8)$$

The plastic process is described by a generalisation of classical plasticity theory that takes into account many aspects of geomaterials' behaviour [11]. The elastic threshold is described by a yield function,

$$F^p(\sigma_{ij}; \kappa^p) = f^p(\sigma_{ij}) - K^p(\sigma_{ij}; \kappa^p) \leq 0 \quad (9)$$

where $f^p(\sigma_{ij})$ is the equivalent stress defined in the stress space. In the general model it can take up the form of any of the yielding functions of classic plasticity (Tresca, Von Mises, Mohr Coulomb, Drucker Prager, etc.). $K^p(\sigma_{ij}; \kappa^p)$ is the yielding threshold and κ^p is the plastic hardening variable.

The Mohr Coulomb yielding surface is used for bricks and mortar and Drucker Prager criterion is used for homogenised masonry in this paper.

The following rule is used for the evolution of plastic strains:

$$\dot{\varepsilon}_{ij}^p = \dot{\lambda} \frac{\partial G(\sigma_{mn}; \kappa^p)}{\partial \sigma_{ij}} \quad (10)$$

where $\dot{\lambda}$ is the plastic consistency factor and G is the plastic potential function. The Mohr Coulomb function is used in this paper as plastic potential function for bricks and mortar and the Drucker Prager function is used for homogenised masonry.

Mohr Coulomb and Drucker Prager functions are yielding criteria defined for isotropic materials. Strength anisotropy and anisotropy orientation of plastic flow are simulated combining these models with the procedure previously described in Section 4.1.1.

The plastic hardening variable κ^p is obtained normalising energy dissipated by the plastic process to unity and varies from 0, for the virgin material, to 1 when the maximum energy is plastically dissipated [10,11].

The damage threshold is described by a damage function in the following way

$$F^d(\sigma_{ij}; \kappa^d) = f^d(\sigma_{ij}) - K^d(\sigma_{ij}; \kappa^d) \leq 0 \quad (11)$$

where $f^d(\sigma_{ij})$ is the equivalent tension, $K^d(\sigma_{ij}; \kappa^d)$ is the equivalent damage threshold and κ^d is the damage hardening variable [11]. It is obtained normalising energy dissipated by damage to unity [11].

The equivalent tension $f^d(\sigma_{ij})$ may be evaluated using known yielding functions (Tresca, Von Mises, Mohr-Coulomb or Drucker-Prager) or any function specially developed for damage [11]. Drucker Prager function is used in this paper to define damage threshold of bricks, mortar and homogenised masonry.

The scalar damage variable d varies from 0 to d_c , that is $0 \leq d \leq d_c$ where $0 < d_c \leq 1$ is the level of damage correspondent to the material failure.

The evolution of permanent strains and damage is obtained from the simultaneous solution of the following equations called the consistency conditions of the problem [11],

$$\begin{cases} \dot{F}^p = 0 \\ \dot{F}^d = 0 \end{cases} \quad (12)$$

Eq. (12) represents two linear equations in $\dot{\lambda}$ and \dot{d} , which can be easily solved.

4.2. CFRP lamina modelling

The reinforcement material made up of polymeric matrix and carbon fibres is itself a composite material formed by a matrix with embedded long fibres. To simplify the numerical simulation and to reduce calculus volume, it is modelled with an equivalent homogeneous macro-model. An orthotropic elasto-plastic model with the composite properties is used for that purpose. The model is similar to that described in Section 4.1 but damage is not activated in this case. Both the orthotropic behaviour inherent to the composite lamina itself and the orthotropic behaviour produced by the weakness of the masonry-CFRP interface are taken into account with this model.

As the properties of the CFRP composite provided by the manufacturer are usually not enough to model this type of material, a generalisation of mixture theory [34,35] is used in the paper to obtain all the remaining mechanical properties. The properties of the composite are obtained from the properties of the fibres and the epoxy matrix and the fibres volume ratio. In this way, the lamina properties already given by the manufacturer are also verified [3].

4.3. CFRP reinforced masonry

The CFRP laminas applied on both faces of the masonry panels are not modelled independently but together with brick, mortar or masonry depending on the modelling approach used. This consideration gives place to a composite material consisting of brick, mortar or masonry and two sheets of composite. In all cases the finite element mesh should be carefully defined so that the elements match the reinforcement zones.

Mixture theory [33] can be used to model the in-plane behaviour of this type of composite where the strains are the same for both component materials. The theory of mixtures is based on the following assumptions [41]: (1) the set of component substances is present in each infinitesimal volume of the composite; (2) each component contributes to the behaviour of the composite

in proportion to its volumetric participation; (3) the volume occupied by each component is lesser than the volume occupied by the composite; and (4) all the components have the same strain. For small strains, this last assumption is written as

$$\varepsilon_{ij} = (\varepsilon_{ij})_1 = (\varepsilon_{ij})_2 = \dots = (\varepsilon_{ij})_n \quad (13)$$

where ε_{ij} and $(\varepsilon_{ij})_n$ represent the strain of the composite and of component n . In the case of CFRP reinforced masonry there are only two component materials that could be bricks + CFRP reinforcement, mortar + CFRP reinforcement or masonry + CFRP reinforcement depending on the approach used and the particular location of the point being modelled.

The strain compatibility assumption described by Eq. (13) constitutes a strong limitation of the theory of mixtures. In particular, the delamination of CFRP laminas represents a strong discontinuity in the strain field inside the composite that cannot be simulated with this theory. When delamination occurs, the stress transfer between the bricks, mortar or masonry and the CFRP is affected and a stress reduction results in the CFRP reinforcement. This stress reduction can be assimilated to a strain reduction related to the interface deformation [32]. This phenomenon can be approximately taken into account in CFRP constitutive model, artificially reducing the shear strength corresponding to the interface plane. With this simplification, the mixture theory can be directly applied to the CFRP reinforced masonry.

The total free energy density per unit volume Ψ of the CFRP reinforced masonry can be written

$$\Psi = k_1 \psi_1 + k_2 \psi_2 \quad (14)$$

where the sub index 1 refers to bricks, mortar or masonry and the sub index 2 refers to CFRP lamina. ψ_i represents the free energy density of each component i , and k_i represents the volume ratio of the component i . In the particular case being modelled, in plane behaviour of CFRP retrofitted masonry, the volume ratios can be directly obtained as thickness ratios.

The secant constitutive equation for the composite results

$$\sigma_{ij} = \frac{\partial \Psi}{\partial \varepsilon_{ij}} = k_1 \frac{\partial \Psi_1}{\partial \varepsilon_{ij}} + k_2 \frac{\partial \Psi_2}{\partial \varepsilon_{ij}} = k_1 (\sigma_{ij})_1 + k_2 (\sigma_{ij})_2 \quad (15)$$

where $(\sigma_{ij})_n$ represents the stress in each of the component materials.

5. Comparison with experimental results

5.1. Introduction

The models described are implemented in a non-linear plane finite element program. A 2D non-linear finite element program developed for research purposes is used for the numerical simulation. Compression perpendicular to the bed joints and diagonal compression tests of unreinforced and CFRP reinforced solid clay masonry panels are simulated with this program. The results of these simulations and their comparison with experimental results [3,4] are hereafter presented.

The behaviour of two similar groups of panels with different dimensions built with bricks of different size is evaluated. The dimensions of the panels were 580 mm × 610 mm × 130 mm and 560 mm × 550 mm × 125 mm and both types of panels had 15 mm-thick mortar joints. The identification of the different specimens tested and the corresponding materials used are presented in Table 1.

The specimens were externally reinforced following two retrofitting schemes: Entire wall reinforcement and reinforcement by means of bands, on both faces. In both cases, a single layer of 1 mm thick composite was applied on each side. In the case of

Table 1
Panels tested [26,27].

Specimen	Group	Retrofitting scheme	Failure load, P_u (kN)	Failure mode
<i>Compression normal to bed joint</i>				
MP3	Ia		286.0	Vertical cracks in front and back sides
MP6	II		216.0	Vertical cracks in front and back sides and crushing near supports
MP7	II		226.0	Vertical cracks in front and back sides and crushing near supports
MP4Ret	Ia	Entirely retrofitted	308.0	Vertical cracks all along the lateral vertical sides
MP5Ret	Ia	Ret. 75 mm width bands	282.0	Small vertical cracks in front, back and lateral sides
MP9Ret	II	Ret. 75 mm width bands	238.0	Small vertical cracks in front, back and lateral sides
<i>Diagonal compression</i>				
MC3	Ib		82.9	Mixed: Bricks failure with joint sliding
MC7	II		85.2	Failure due to diagonal tensions and sliding
MC4Ret	Ib	Entirely retrofitted	246.2	Crushing in support zone
MC5Ret	Ib	Ret. 50 mm width bands \perp load	145.6	Bricks failure near supports
MC6Ret	Ib	Ret. 50–60 mm width bands//bed joints	88.3	Bricks failure near supports with sliding of central mortar joint

Ret: Retrofitted.

Table 2
Brick and mortar mechanical properties.

Specimens Properties	Group I: 580 × 610 × 130 (mm ³)			Group II: 560 × 550 × 125 (mm ³)	
	Mortar (a)	Mortar (b)	Brick	Mortar	Brick
Elasticity modulus, E (MPa)	3380	4312	1662	1528	1400
Poisson's ratio, ν	0.21	0.21	0.16	0.21	0.15
Tension ultimate strength, σ_{ut} (MPa)	0.673	0.772	0.591	0.54	0.414
Compression ultimate strength, σ_{uc} (MPa)	6.73	7.72	10.60	4	8.28
Uniaxial compression elastic threshold, σ_{fc} (MPa)	5.60	6.4	–	3.5	–
Initial compression/tension strength ratio, R_0^p	10	10	20	10	20
Plastic damage variable for the peak stress, κ_{comp}^p	0.20	0.20	–	0.20	–
Fracture energy, G_f^p (MPa m)	6.0E–5	4.0E–5	3.0E–5	1.0E–5	3.0E–5
Crushing energy, G_c^p (MPa m)	6.0E–3	4.0E–3	2.0E–3	1.0E–3	2.0E–3
Yield criterion	Mohr Coulomb	Mohr Coulomb	Drucker Parger	Mohr Coulomb	Drucker Parger
Plastic flow	Mohr Coulomb	Mohr Coulomb	Drucker Parger	Mohr Coulomb	Drucker Parger
Shear strength ratio in mortar plane (τ/σ in Eq. (2))	3	3	1	3	1
Damage criteria	Drucker–Prager	Drucker–Prager	Drucker–Prager	Drucker–Prager	Drucker–Prager
Friction angle for damage function ($^\circ$)	7	7	7	7	7
Uniaxial compression damage threshold, σ_{dc} (MPa)	5.9	7.0	10	3.7	7.5
Damage crushing energy, G_c^d (MPa m)	6.0E–3	6.0E–3	5.0E–2	6.0E–3	5.0E–2
Damage fracture energy, G_f^d (MPa m)	2.0E–5	2.0E–5	2.0E–4	2.0E–5	2.0E–4

the specimens subjected to compression normal to bed joints, the bands were located parallel to bed joints with the fibres in the same direction. The same retrofitting scheme and another with the bands orthogonal to load direction were used in the case of the panels subjected to diagonal compression. See Table 1.

Masonry is modelled analysing the bricks and the mortar separately. For both materials, orthotropic models with damage combined with plasticity are used [3]. The mechanical properties of mortars and bricks used for the model were obtained from tests and are summarised in Table 2 [3,4]. Elasticity modulus, Poisson's ratio, compression ultimate strength, uniaxial compression elastic threshold, plastic damage variable for the peak stress, crushing energy, uniaxial compression damage threshold, were obtained from uniaxial compression tests while mortar initial compression/tension strength ratio and fracture energy were obtained from notched beam flexure tests. The rest of the functions and properties defining material behaviour (yield criterion, plastic flow criterion, damage criterion and the parameters used to defined them) were proposed as those commonly used for this type of materials and validated with experimental results of unreinforced masonry small specimens tested under compression and diagonal compression. The results of a series of experimental tests on small masonry units made of three bricks and two mortar joints and tested them under shear [16] were used to calibrate the ratio between shear strength in the isotropic fictitious space and the actual shear strength in joint planes used in Eq. (2) (Table 2).

The mechanical properties of CFRP lamina are presented in Table 3.

All the specimens are modelled with three node triangular plane stress finite elements. Some tests were also done with four node rectangular finite elements. The results show a stiffness over-estimation in the last case. This is due to the impossibility of maintaining a suitable aspect ratio for the rectangular finite elements that matches the joints and the bricks geometry.

5.2. Compression normal to the bed joints

The behaviour of solid clay masonry panels subjected to compression perpendicular to the bed joints is studied in this section. Some of them have no reinforcement and others are retrofitted with CFRP laminates according to different schemes. See Table 1.

5.2.1. Unreinforced panels

The test setup, the finite elements mesh, boundary and loading conditions for masonry panels tested under compression normal to the bed joints are presented in Fig. 1. Taking advantage of the specimen symmetry only a quarter is modelled. Load-axial and transversal displacement curves ($P-\delta_l$ and δ_t) for both types of walls are presented in Fig. 2. Displacements represented correspond to total vertical and horizontal relative displacements of the panels' sides. A better adjustment of the experimental results in the axial direction can be observed. Actually, discrete cracks located at

Table 3
Composite mechanical properties.

Volume fraction of fibres, k_f	0.3
Longitudinal elasticity modulus, E_l (MPa)	72,500
Transversal elasticity modulus, E_t (MPa)	6200
Longitudinal–transversal Poisson's ratio, ν_{lt}	0.08
Transversal–longitudinal Poisson's ratio, ν_{tl}	0.017
Transversal–transversal Poisson's ratio, ν_{tt}	0.20
Longitudinal tensile strength, σ_{long}^u (MPa)	960
Transverse tensile strength, σ_t^u (MPa)	51
Yield criterion	Tresca

certain positions appeared in the tests. The continuum constitutive model used considers the cracking distributed all along the width of the panel and so it is not able to accurately reproduce transverse deformation. The failure deformation in transverse direction numerically obtained is always much lower than that obtained in the tests. Nevertheless, initial stiffness in axial and transverse directions, strength and maximum axial deformation are approximately reproduced. The experimental and numerical values of the failure load, initial stiffness in axial direction and maximum axial displacement corresponding to three unreinforced specimens (MP3, MP6 and MP7), are presented in Table 4. The relative differences between numerical and experimental results are also included in Table 4. The maximum difference obtained for failure loads is about 5.6% while the maximum differences for initial stiffness and maximum displacement are 15.4% and 63.6%, respectively. A good prediction of maximum displacement was achieved for specimens MP3 and MP7 but not for specimen MP6. Although specimens MP6 and MP7 were similar, maximum displacement achieved by specimen MP6 was sensibly lower. The difference observed in the tests was probably due to some local defects that caused a premature failure in the case of specimen MP6. This type of problem cannot be taken into account with the numerical model that gives exactly the same results for both specimens.

5.2.2. CFRP reinforced panels

The behaviour of solid clay unit panels reinforced with CFRP sheets is simulated. Finite element mesh boundary and loading conditions are presented in Fig. 3. Since the panels are symmetric, a quarter of them is modelled too.

The load–axial and transverse displacement curves obtained for reinforced panels are contrasted with the experimental results in Fig. 4. In the case of the entirely reinforced specimen, due to problems in the measurement system, only the axial displacements were recorded.

In general, a good correlation with experimental results is observed with respect to maximum load and initial stiffness. The experimental and numerical values of the failure load, initial stiffness in axial direction and maximum axial displacement corresponding to three retrofitted specimens (MP4Ret, MP5Ret and MP9Ret), are presented in Table 4. The relative differences between numerical and experimental results are also included in Table 4. The maximum difference obtained for failure load is about 2.3%, while the maximum differences for initial stiffness and maximum displacement are 7.3% and 20.6% respectively.

The maximum load under compression normal to bed joint is not incremented by the FRP retrofitting technique. It can be proved that, whatever the strip width is, even in the case of the entirely reinforced panel, the strength is not increased [4]. Failure is defined by masonry failure since CFRP laminas are debonded and due to their reduced thickness they can no longer bear external load without buckling. Failure load can be approximately obtained as the sum of the contributions provided by masonry and CFRP lamina at failure. CFRP lamina is oriented with the fibres orthogonal to load direction. As a result of the low stiffness of the reinforcement in vertical direction and the reduced thickness of the lamina, the contribution to the vertical strength is negligible.

It was found that the reinforcement has no effect on initial stiffness of the masonry wall, in spite of composite strips width (see Table 4). For the totally retrofitted wall, initial vertical thickness can be approximately obtained as the sum of masonry and CFRP laminas stiffness, each one multiplied by its corresponding relative cross sectional area (cross sectional area/cross sectional area of the retrofitted masonry wall). As a result of the low stiffness of the reinforcement in vertical direction and the reduced thickness of the lamina, even in this case, the contribution of CFRP laminas to the vertical stiffness is negligible. The contribution of CFRP bands to vertical stiffness is even smaller but the difference with the lamina covering the whole wall surface is very little.

An increase in axial deformation capability of about 240% was obtained for the totally reinforced panel while this increase is 12% and 22% for the specimens reinforced with strips compared with unreinforced panel. Total reinforcement acts like a lateral passive confinement, preventing the opening of vertical cracks. Lateral compression stresses appeared and the change in stress state gives place to a vertical ductility increase. In the case of CFRP bands the vertical continuity is interrupted and this confinement effect is only locally achieved and thus the effect on vertical ductility is lower.

The failure mode of the CFRP reinforced panels is totally modified with respect to an unreinforced specimen. While vertical cracks through mortar joints and bricks developed on the front

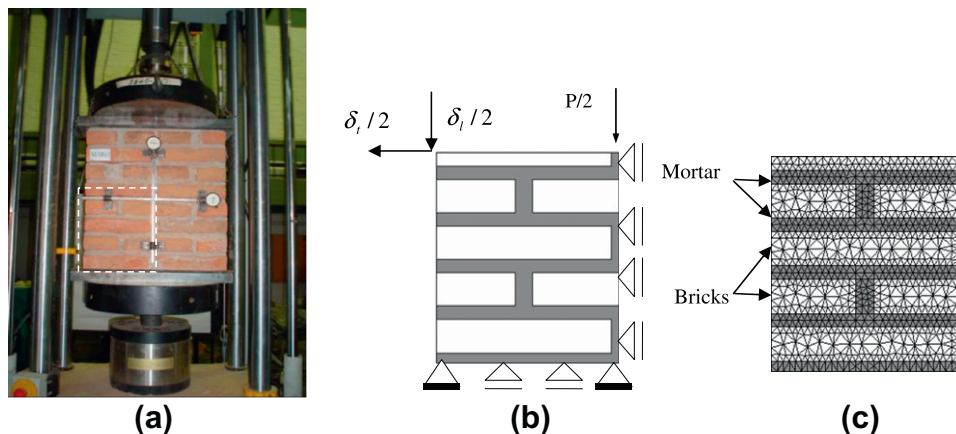


Fig. 1. Unreinforced panel under compression normal to bed joints: (a) test setup, (b) load and boundary conditions, (c) finite element mesh.

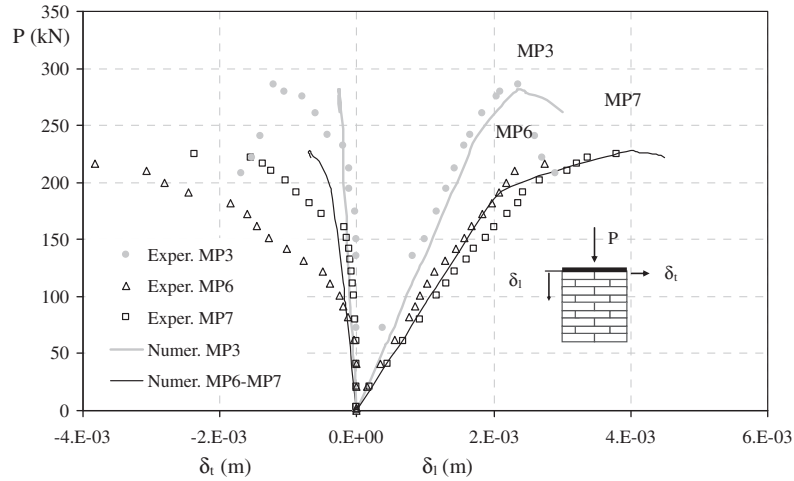


Fig. 2. Axial load versus axial and transverse displacement diagrams for unreinforced panels under compression normal to the bed joints.

Table 4
Compression normal to bed joints. Comparison of numerical and experimental results.

Results	MP3	MP6	MP7	MP4Ret	MP5Ret	MP9Ret
P_{max} experim. (kN)	286	216	226	308	282	238
P_{max} numer. (kN)	281	228	228	315	285	240
Difference %	-1.8	5.6	0.9	2.3	1.1	0.8
K experim. (kN/mm)	148.6	96.5	81.1	151.5	135.3	99.0
K numer. (kN/mm)	137.5	93.5	93.5	147.0	145.2	100.7
Difference %	-7.5	-3.1	15.4	-3.0	7.3	1.8
δ_m Experim. (mm)	2.9	2.8	3.8	4.4	3.4	3.9
δ_m Numer. (mm)	3.0	4.5	4.5	5.0	2.7	4.3
Difference %	3.3	63.6	19.0	12.2	-20.6	10.5

P_{max} : Maximum load.
 K : Initial vertical stiffness.
 δ_m : Maximum vertical displacement.
 Difference = 100(Numer-Exper)/Exper.

and back faces of unreinforced specimens, vertical cracks on their sides and a more ductile behaviour depending on the reinforcement configurations adopted, are observed in retrofitted panels. It can be proved that the vertical deformation capacity is notably increased when the strip width increases [4]. This improvement is due to the action of the fibres preventing brittle opening of vertical cracks, and increases with strip width.

Transverse displacements are more accurately simulated than in the case of unreinforced panels. The overall behaviour and particularly, the failure mode characterised by crushing in the support zone for the entirely reinforced panel can be properly reproduced by the numerical model.

5.3. Diagonal compression

In this section, the in-plane shear behaviour under diagonal compression of solid clay masonry panels without reinforcement

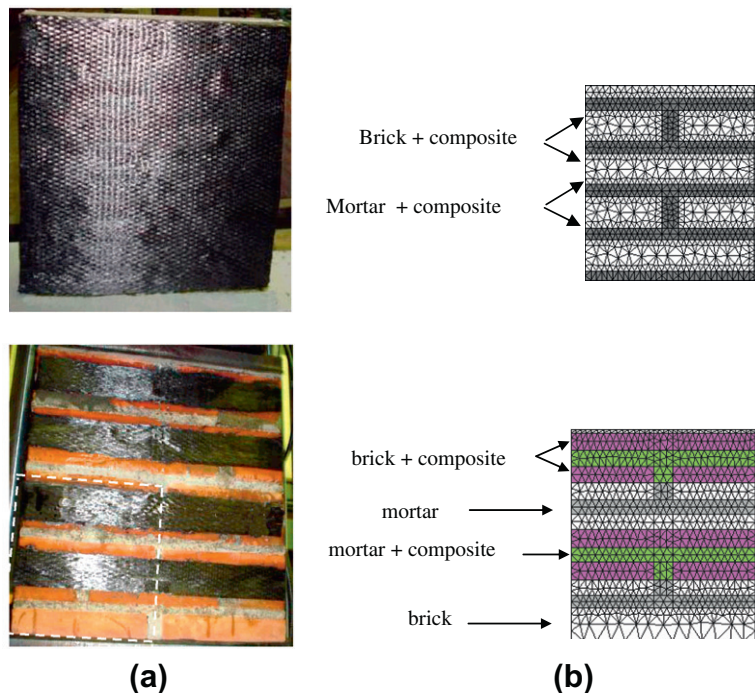


Fig. 3. CFRP strips retrofitted panel (a) Panels tested, (b) finite element mesh.

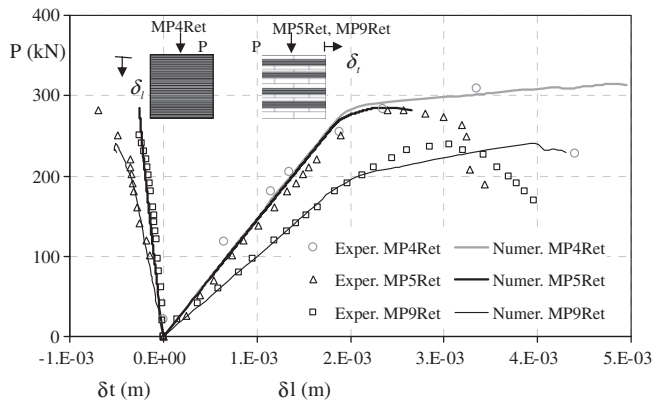


Fig. 4. Axial load versus axial and transverse displacement curves for compression normal to the bed joints of CFRP retrofitted panels.

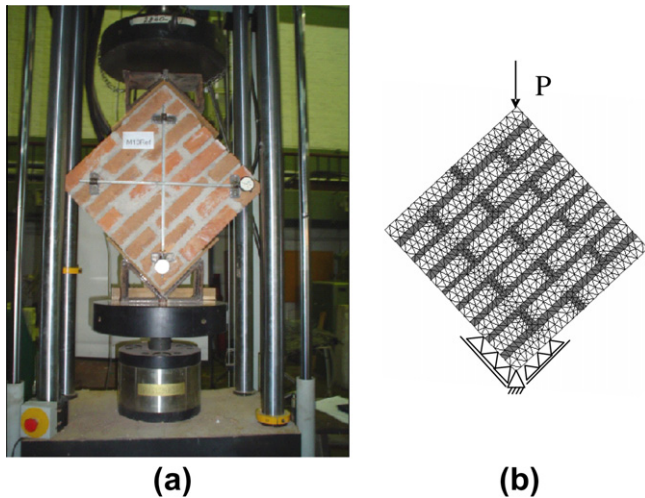


Fig. 5. Unreinforced panel under diagonal compression: (a) test setup; (b) finite element mesh.

and reinforced with CFRP sheets is simulated. Numerical results are compared with experimental results.

5.3.1. Unreinforced panels

The finite elements mesh and the loading conditions for this type of test are presented in Fig. 5. The whole panel is modelled in this case. The evolution of transverse and longitudinal displacements (δ_t and δ_l) as a function of the applied load for specimens MC3 and MC7 (see Table 1) is presented in Fig. 6. Numerical results are close to experimental response in vertical direction and differ in the case of transverse direction for which the deformation is a result of a combination of different complex mechanisms. The model properly reproduces not only the strength but also the brittle failure mechanism without excessive previous deformation. The response curves are approximately bilinear with both elastic and inelastic stiffness closed to experimental results.

The experimental and numerical values of the failure load, initial stiffness in diagonal direction and maximum diagonal displacement corresponding to two unreinforced specimens (MC3 and MC7) are presented in Table 5. The relative differences between numerical and experimental results are also included in Table 5. The maximum difference obtained for failure loads is about 4.0% while the maximum differences for initial stiffness and maximum displacement are 32.0% and 10.3% respectively.

5.3.2. CFRP reinforced panels

The finite element meshes used for the reinforced specimens are shown in Fig. 7. The load–displacement curves, through the compressed and stretched diagonals of the panel, for different retrofitting setups are presented in Fig. 8.

The model reasonably reproduces the global behaviour of retrofitted specimens under diagonal compression and strength is accurately predicted. The use of a mortar with lower shear strength in joint planes allows reproducing the brittle failure characterised by joint sliding. The behaviour is less brittle than for unreinforced specimens and the predicted increase in ultimate strength is close to that obtained in the tests.

The experimental and numerical values of the failure load, initial stiffness in diagonal direction and maximum diagonal displacement corresponding to three retrofitted specimens (MC4Ret, MC5Ret and MC6Ret) are presented in Table 5. The relative differences between numerical and experimental results are also included in Table 5. The maximum difference obtained for failure loads is about 7.0% while the maximum differences for initial stiffness and maximum displacement are 16.2% and 13.6% respectively.

It can be seen that the reinforcement with strips placed parallel to bed joints (at 45° with respect to load direction) does not improve the behaviour of the masonry element. A localised effect in the upper support that causes the failure of the superficial layers of the bricks producing the debonding of composite bands applied in this area is observed in this type of test. In consequence, if the central mortar joint is not reinforced, the specimen fails due to joint sliding. This type of failure is sudden and it takes place under low load values.

Fig. 8 shows that total reinforcement significantly increases the stiffness and the strength of the panel, preventing joints sliding. Due to the action of CFRP lamina, the integrity of the specimen is preserved without evidence of cracks near to failure load. Failure is produced by the brick crushing near the upper support.

In contrast, no appreciable increase in stiffness is obtained with diagonal strips but, as it can be observed in Fig. 8, the ultimate load is practically duplicated with a significant saving of CFRP material. Diagonal CFRP bands preserve panel integrity but specimen failure takes place due to detachment of the superficial layers of the bricks. This failure is initiated near the upper support and propagates to the lower support.

6. Behaviour of a CFRP reinforced masonry wall

The behaviour of masonry walls, retrofitted with CFRP and subjected to quasi-static cyclic lateral load [8] is simulated in this section. The objective of this numerical study is to prove the ability of the described model to quantify the improvement in the in plane shear strength of masonry walls of actual dimensions, CFRP reinforced according to different configurations and with different reinforcement quantities.

The dimensions of the walls made of hollow clay bricks are shown in Fig. 9. They had a bottom and a top reinforced concrete transfer beam with nominal dimensions of 2260 mm × 300 mm × 400 mm and 2260 mm × 325 mm × 400 mm; bottom and top. Two grouted 25 mm diameter steel bars with 420 MPa yield stress were placed at the wall ends [8].

The specimens were reinforced with CFRP on both sides according to different schemes: no reinforcement (NSRM), 3 horizontal strips 100 and 150 mm (HSRM-3 × 100 and HSRM-3 × 150); one horizontal strip 300 mm wide (HSRM-1 × 300); one pair of 200 and 300 mm wide diagonal strips (DSRM-1 × 200 and DSRM-1 × 300) and three pairs of 100 mm wide diagonal strips (DSRM-1 × 300). For the horizontal strips, composite material was applied

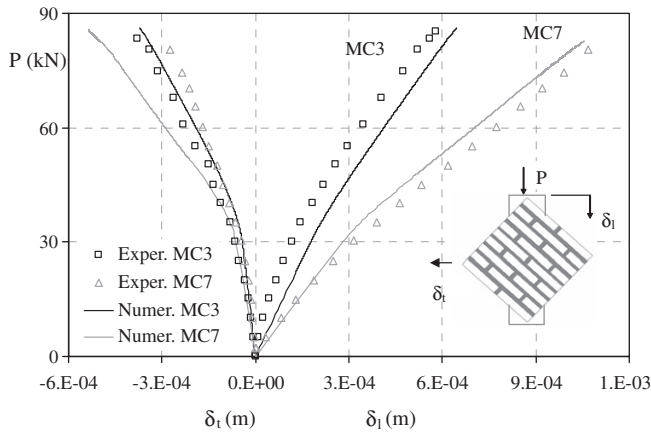


Fig. 6. Load–displacement diagram of the compressed and stretched diagonals of unreinforced panels.

Table 5
Diagonal compression. Comparison of numerical and experimental results.

Results	MC3	MC7	MC4Ret	MC5Ret	MC6Ret
P_{max} experim.(kN) exp.	82.9	85.2	246.2	145.6	88.3
P_{max} numer. (kN)	86.2	82.7	229.0	147.3	84.0
Difference %	4.0	-2.9	-7.0	1.2	-4.9
K experim (GPa)	250.0	106.4	141.1	146.3	165.5
K numer. (GPa)	170.0	108.8	163.9	146.8	162.5
Difference %	-32.0	2.3	16.2	0.3	-1.8
δ_m Experim. (mm)	0.58	1.07	2.32	1.50	0.59
δ_m Numer. (mm)	0.64	1.05	2.31	1.38	0.67
Difference %	10.3	-1.9	-0.4	-8.0	13.6

P_{max} : Maximum load.
 K : Initial diagonal stiffness.
 δ_m : Maximum diagonal displacement.
 Difference = 100(Numer-Exper)/Exper.

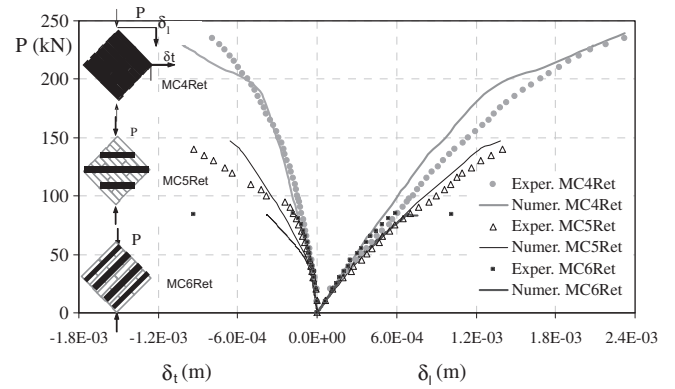


Fig. 8. Load versus axial and transverse displacement curves for panels with different CFRP retrofitting schemes under diagonal compression.

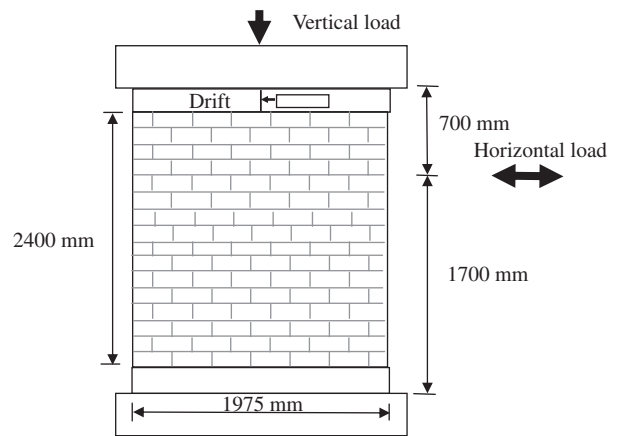


Fig. 9. CFRP reinforced walls: Dimension and loading conditions.

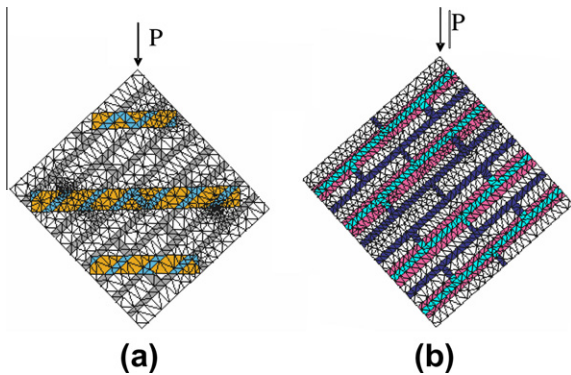


Fig. 7. CFRP retrofitted panels-finite element mesh: (a) retrofitting with strips orthogonal to load direction, (b) retrofitting with strips parallel to bed joints.

with fibres in horizontal direction while for diagonal strips the fibres were applied in diagonal direction.

The walls were subjected to in-plane controlled displacement cyclic loading, in conjunction with a constant vertical load of approximately 98 kN. The walls were fixed to the floor but were left free to laterally displace and rotate at the top. The load was applied at a distance of 1700 mm from the top of the bottom transfer beam. See Fig. 9.

Due to the size of the wall simulated, masonry is modelled using only one equivalent orthotropic material. The main material

properties used for masonry, concrete and steel and CFRP reinforcement were obtained from Ref. [8] and are presented in Tables 6 and 7. The remaining properties of masonry were obtained by fitting the response of the unreinforced wall with experimental results.

Loading and boundary conditions, retrofitting schemes and finite element meshes are shown in Fig. 10. Plane stress triangular finite elements are used and the complete walls are modelled. The load transmission frame was idealised through a stiff steel arm because the actual dimensions were not available in Ref. [8].

Lateral load versus lateral displacement curves for the unreinforced and reinforced walls under cyclic lateral load are presented in Fig. 11. The shape of these hysteretic curves is similar to those obtained in the tests [8], showing permanent deformation and increasing stiffness degradation. The loops are narrower in the case of retrofitted walls.

The comparison of the numerical load displacement envelope curves and experimental envelope curves for the first cycles is presented in Fig. 12. The differences between the first and the second displacement cycles are not important up to a displacement 5 mm but the differences are more evident for greater displacements (see Fig. 11). In general, a good agreement between numerical and experimental results is observed in Fig. 12. Numerical initial stiffness is slightly greater than that obtained in the tests. The differences could be attributed to the assumption of masonry as a continuous homogeneous material and ideal supports conditions in the numerical model. The peak load is approximately reproduced while differences in the post-peak curve can be observed

Table 6
Masonry, concrete and steel properties [16].

Material	Masonry	Concrete	Steel
Elasticity modulus, E (MPa)	6618	22,000	210,000
Poisson's ratio, ν	0.287	0.2	0.3
Tension ultimate strength, σ_{ut} (MPa)	0.56	3.0	400
Compression ultimate strength, σ_{uc} (MPa)	11.3	35	400
Uniaxial compression elastic threshold, σ_{fc} (MPa)	7.00	30	400
Initial compression/tension strength ratio, R_p^0	12.5	10	1
Plastic damage variable for the peak stress, κ_{comp}^p	0.20	0.20	
Fracture energy, G_f^p (MPa m)	5.0E-3	1.0E-3	
Crushing energy, G_c^p (MPa m)	5.0E-2	7.0E-2	
Yield criterion	Drucker–Prager	Mohr Coulomb	Von Mises
Plastic flow	Drucker–Prager	Mohr Coulomb	Von Mises
Damage criteria	Drucker–Prager		
Uniaxial compression damage threshold, σ_{dc} (MPa)	8.0		
Damage fracture energy, G_f^d (MPa m)	2.5E-3		
Damage crushing energy, G_c^d (MPa m)	5.0E-2		

Table 7
CFRP properties [16].

Unidirectional carbon fibre sheet thickness (mm)	0.13
Composite lamina thickness (mm)	1.00
Carbon fibre sheet longitudinal elasticity modulus, E_l (MPa)	250,000
Carbon fibre sheet longitudinal tensile strength, σ_{long}^t (MPa)	4300
Yield criterion	Tresca

for some cases but scattering of experimental results for this range have also been observed [8].

As in the tests, the failure of the non-retrofitted wall is brittle and the maximum lateral load of 125 kN corresponds to a drift of approximately 5 mm. All retrofitted walls are able to sustain great-

er lateral load cycles than the non-retrofitted walls but shear strength numerically obtained is slightly lower than that obtained in the tests. The maximum drift obtained in the tests, 10–12 mm for the horizontal reinforcement and 12–14 mm for the diagonal reinforcement, is also reproduced. The behaviour of the walls reinforced with only one strip is more brittle than that of the walls retrofitted with three strips. As in the tests, the walls retrofitted with three bands have a residual strength that makes them able to reach greater lateral displacement before failure. Due to vertical reinforcement bars, failure of the panels is mainly a shear failure. As a consequence, a greater increase in shear strength is obtained with the diagonal CFRP reinforcement but considering the ratio

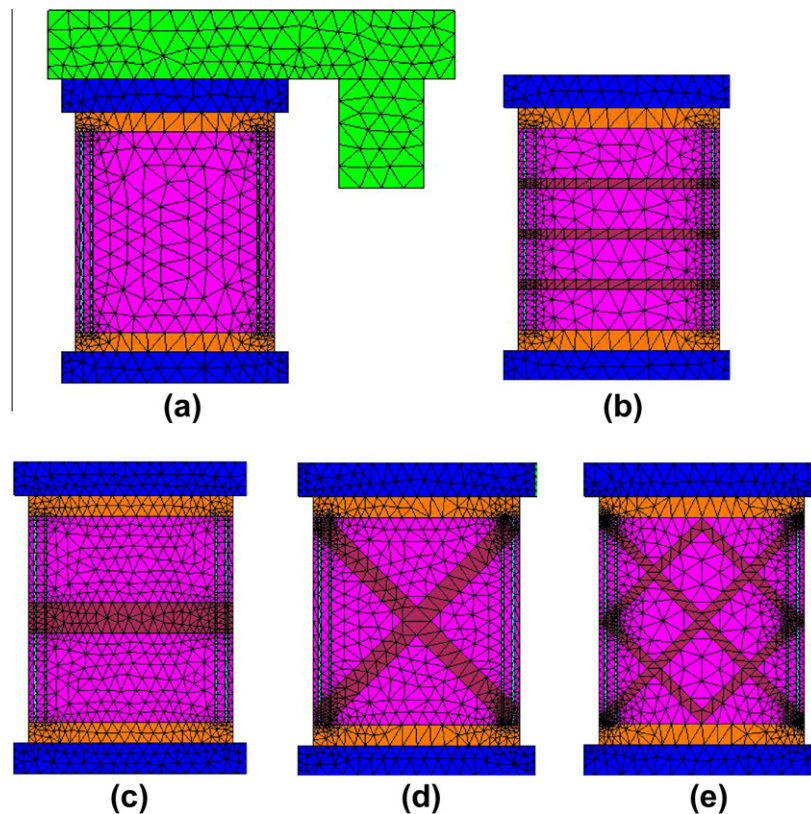


Fig. 10. CFRP reinforced walls. Retrofitting schemes and finite element mesh. (a) Unreinforced wall (NSRM), (b) wall retrofitted with three horizontal CFRP strips (HSRM-3 × 100), (c) wall retrofitted with one horizontal CFRP strip (HSRM-1 × 300), (d) wall retrofitted with one pair of diagonal strips (DSRM-1 × 200), (e) wall retrofitted with three pairs of diagonal strips (DSRM-3 × 100).

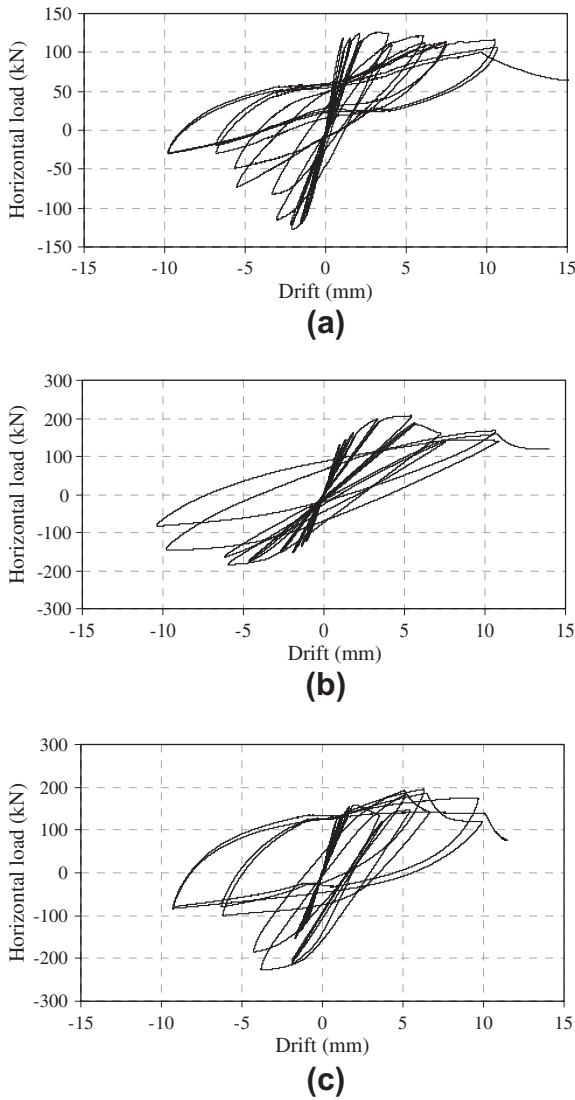


Fig. 11. CFRP retrofitted masonry walls under cyclic load. Load versus lateral displacement curves. (a) NSRM, (b) HSRM-3 × 150, (c) DSRM 1 × 200.

strength increase/area of reinforcement, horizontal reinforcement is more efficient [19].

The comparison with the experimental results by Alcaino and Santa María [8] show that the model is able to reproduce the behaviour of retrofitted masonry panels not only under simple load cases like those shown in the previous section but also under combined compression and shear. Moreover, these results prove the ability and robustness of the model to simulate cyclic loading capturing the hysteretic response of the panels tested. For unreinforced masonry, the shape of the numerical hysteresis loops is mainly dependent on masonry plasticity and damage parameters. When the panels are retrofitted with CFRP bands, the contribution of this material modifies the shape of the overall hysteresis curves. As the model used is a continuous model, crack pattern cannot be explicitly captured but overall damaged response and failure is properly reproduced.

7. Conclusions

Due to the cost, extension and complexity that experimental programs may have, it is important to have a numerical tool to satisfactorily reproduce the behaviour of FRP retrofitted masonry un-

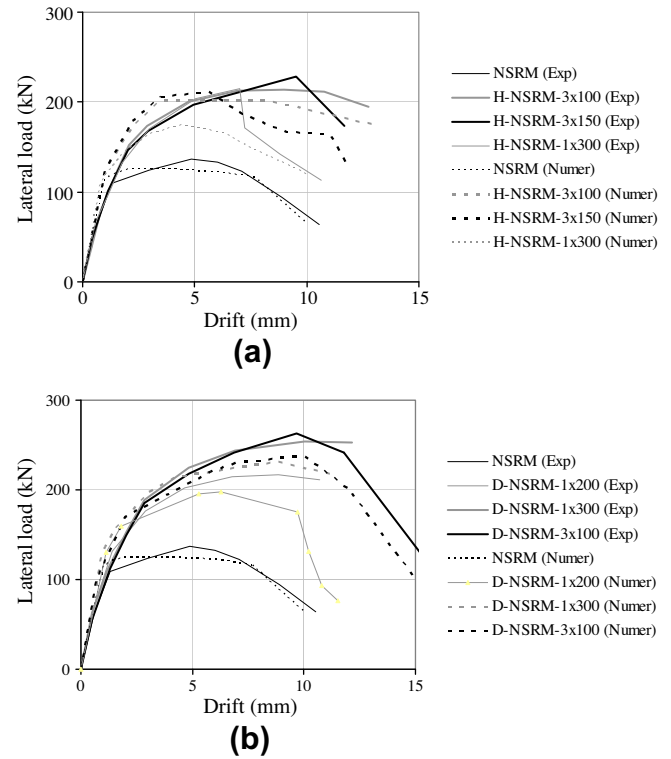


Fig. 12. Envelope load versus lateral displacement for masonry walls retrofitted with CFRP using different retrofitting schemes. (a) Horizontal reinforcement and (b) diagonal reinforcement.

der different in plane stress states. Once the model has been adjusted, a numerical study allows the analysis of different loading conditions and repair or reinforcement assemblages, which means a smaller number of laboratory tests.

A numerical model for the analysis of CFRP reinforced masonry is presented in this paper. CFRP retrofitted masonry is simulated as a composite material made in turn of composites. A simple approach based on mixture theory, which allows the analysis of the behaviour of CFRP reinforced masonry from the properties of the constitutive materials and their particular arrangement, without explicitly modelling the reinforcement is used.

An anisotropic plastic damage model is used to simulate the behaviour of bricks, mortar and CFRP reinforcement. In this way, the behaviour under monotonic and cyclic loads characterised by permanent deformations and stiffness degradation can be properly reproduced. The interfaces between the different constituents are not explicitly modelled but are indirectly taken into account in the constitutive laws of each of the materials with consequent reduction in computational cost.

In general, the numerical model used is able to reproduce the values of maximum load and stiffness of unreinforced and CFRP reinforced masonry panels. For unreinforced masonry subjected to compression normal to the bed joints, it is possible to get a good prediction of axial displacements, but not of transverse displacements.

From the numerical study performed, it can be concluded that under compression normal to the bed joints, the reinforcement with FRP strips increases neither the masonry strength nor the stiffness. However, an increase in the deformation capacity can be obtained with a wide strip. For specimens under diagonal compression, the diagonal FRP reinforcement increases both the strength and the deformation capacity.

The results of the simulation of unreinforced and CFRP retrofitted masonry walls under constant vertical load and cyclic lateral

load show that this retrofitting technique can improve shear strength and ductility and the improvement increases with the amount of reinforcement. As already proved experimentally [19], horizontal reinforcement is more effective than diagonal reinforcement in terms of maximum load capacity increase/amount of reinforcement ratio.

In spite of the simplifications used to model actual dimension masonry panels, a reasonable agreement between experimental and numerical results is obtained showing that an equivalent homogeneous anisotropic damage model can be used to model actual masonry elements with a great save of computational cost. Moreover CFRP reinforcement can be simply accounted for using mixture theory.

Acknowledgments

The financial support from CONICET, CIUNT, National University of Tucumán and Technological University is gratefully acknowledged. The authors also wish to thank Ings. Jorge Rendón and Paulino Maldonado, from Sika Colombia and Sika Argentina, respectively, for composite material donations, to carry out experimental tests and the collaboration of Ms. Viviana Kay and Ms. Amelia Campos in the English revision.

References

- [1] ElGawady M. Seismic retrofit of URM walls with fiber composites. PhD thesis, IS-IMAC, EPFL, Switzerland; 2004.
- [2] Valluzzi MR, Tinazzi D, Modena C. Shear behavior of masonry panels strengthened by FRP laminates. *Constr Build Mater* 2002;16:409–16.
- [3] Rougier V. Refuerzo de muros de mampostería con materiales compuestos. PhD Thesis, Structures Institute, Nacional University of Tucumán, Argentina; 2007.
- [4] Luccioni B, Rougier V. In-plane retrofitting of masonry panels with fiber reinforced composite materials. *Constr Build Mater* 2011;25(4):1772–88.
- [5] ElGawady MA, Lestuzzi P, Badoux M. A seismic retrofitting of unreinforced masonry walls using FRP. *Composites: Part B* 2006;37:148–62.
- [6] Marcarì G, Manfredi G, Prota A, Pecce M. In-plane shear performance of masonry panels strengthened with FRP. *Composites: Part B* 2007;38:887–901.
- [7] Santa María H, Alcaino P, Luders C. Experimental response of masonry walls externally reinforced with carbon fiber fabrics. In: *Proceedings of the 8th U.S. National Conference on Earthquake Engineering*, San Francisco, California, USA; 2006.
- [8] Alcaino P, Santa María H. Experimental response of externally retrofitted masonry walls subjected to shear loading. *J Compos Constr* 2008;12(5):489–98.
- [9] Luccioni B, Oller S, Danesi R. Plastic damaged model for anisotropic materials. *Appl Mech Eng* 1995;1:124–9.
- [10] Luccioni B, Rougier V. A plastic damage approach for confined concrete. *Comput Struct* 2005;83:2238–56.
- [11] Luccioni B, Oller S, Danesi R. Coupled plastic-damaged model. *Comput Methods Appl Mech Eng* 1996;129:81–9.
- [12] El-Dakhkhni W, Hamid A, Hakam Z, Elgaaly M. Hazard mitigation and strengthening of unreinforced masonry walls using composites. *Compos Struct* 2006;73(4):458–77.
- [13] Prakash S, Alagusundaramoorthy P. Load resistance of masonry wallettes and shear triplets retrofitted with GFRP composites. *Cem Concr Compos* 2008;30(8):745–61.
- [14] Zhuge H. FRP-retrofitted URM walls under in-plane shear: review and assessment of available models. *J Compos Constr* 2010;14(6):743–53.
- [15] Roca P, Araiza G. Shear response of brick masonry small assemblages strengthened with bonded FRP laminates for in-plane reinforcement. *Constr Build Mater* 2010;24:1372–84.
- [16] Luccioni B, Rougier V. Shear behaviour of brick mortar interface in CFRP retrofitted or repaired masonry. *Int J Mech Sci* 2010;52:602–11.
- [17] Gabor A, Bennani A, Jacquelin E, Lebon F. Modelling approaches of the in-plane shear behaviour of unreinforced and FRP strengthened masonry panels. *Compos Struct* 2006;74:277–88.
- [18] ElGawady M, Lestuzzi P, Badoux M. In-plane seismic response of URM walls upgraded with FRP. *J Compos Constr* 2005;9(6):524–35.
- [19] ElGawady MA, Lestuzzi P, Badoux M. Static cyclic response of masonry walls retrofitted with fiber-reinforced polymers. *J Compos Constr* 2007;11(1):50–61.
- [20] Santa María H, Alcaino P. Repaired of in-plane shear damaged masonry walls with external FRP. *Constr Build Mater* 2011;25:1172–80.
- [21] Chuang S, Zhuge Y, Wong T, Peters L. Seismic retrofitting of unreinforced masonry walls by FRP strips. *Pacific conference on earthquake engineering*; 2003.
- [22] Prota A, Manfredi G, Nardone F. Assessment of design formulas for in-plane FRP strengthening of masonry walls. *J Compos Constr* 2008;12(6):643–9.
- [23] Shrive NG. The use of fibre reinforced polymers to improve seismic resistance of masonry. *Constr Build Mater* 2006;20:269–77.
- [24] Papanicolaou C, Triantafyllou T, Lekka M. Externally bonded grids as strengthening and seismic retrofitting materials of masonry panels. *Constr Build Mater* 2011;25(2):504–14.
- [25] Ehsani M, Saadatmanesh H, Al-Saidy A. Shear behavior of URM retrofitted with FRP overlays. *J Compos Constr* 1997;1(1):17–25.
- [26] Cecchi A, Milani G, Tralli AY. In-plane loaded CFRP reinforced masonry walls: mechanical characteristics by homogenization procedures. *Compos Sci Technol* 2005;65:1480–500.
- [27] Gabor A, Ferrier E, Jacquelin E, Hamelin P. Analysis and modelling of the in-plane shear behaviour of hollow brick masonry panels. *Constr Build Mater* 2006;20:308–21.
- [28] Grande E, Milani G, Sacco E. Modelling and analysis of FRP-strengthened masonry panels. *Eng Struct* 2008;30:1842–60.
- [29] Fedele R, Milani G. A numerical insight into the response of masonry reinforced by FRP strips. The case of perfect adhesion. *Compos Struct* 2010;92:2345–57.
- [30] Milani G, Milani E, Tralli A. Approximate limit analysis of full scale FRP-reinforced masonry buildings through a 3D homogenized FE package. *Compos Struct* 2010;92:918–35.
- [31] Su Y, Wu C, Griffith M. Modelling of the bond–slip behavior in FRP reinforced masonry. *Constr Build Mater* 2011;25(1):328–34.
- [32] Luccioni B, López D, Danesi R. Bond slip in reinforced concrete elements. *J Struct Eng – ASCE* 2005;131(11):571–4.
- [33] Oller S, Oñate E, Miquel J, Botello S. A plastic damage constitutive model for composite materials. *Int J Solids Struct* 2006;33(17):2501–18.
- [34] Luccioni B. Constitutive model for fiber reinforced composite laminates. *J Appl Mech* 2006;73(6):901–10.
- [35] Toledo M, Nallim L, Luccioni B. A micro–macromechanical approach for composite laminates. *Mech Mater* 2008;40:885–906.
- [36] Betten J. Application of tensor functions to the formulation of yield criteria for anisotropic materials. *Int J Plast* 1988;4:29–46.
- [37] Oller S, Botello S, Miquel M, Oñate E. Anisotropic elasto–plastic model based on an isotropic formulation. *Eng Comput* 1995;12:245–62.
- [38] Luccioni B, Martín P. Modelo elastoplástico para materiales ortótropos. *Rev Int Mét Num Dis Cálculo* 1997;13(4):603–61.
- [39] Car E, Oller S, Oñate E. A large strain plasticity model for anisotropic composite material application. *Int J Plast* 1999;17(11):1437–63.
- [40] Oller S, Car E, Lubliner J. Definition of a general implicit orthotropic yield criterion. *Comput Meth Appl Mech Eng* 2003;192:895–912.
- [41] Truesdell C, Toupin R. The classical field theories. In: *Flügge S, editor. Handbuch der Physik II/I*. Berlin: Springer; 1960.